



Universiteit  
Leiden  
The Netherlands

## Development and testing of the gravitational wave antenna MiniGRAIL in its full-featured configuration

Usenko, O.

### Citation

Usenko, O. (2012, May 23). *Development and testing of the gravitational wave antenna MiniGRAIL in its full-featured configuration*. *Casimir PhD Series*. Retrieved from <https://hdl.handle.net/1887/18979>

Version: Not Applicable (or Unknown)

License: [Leiden University Non-exclusive license](#)

Downloaded from: <https://hdl.handle.net/1887/18979>

**Note:** To cite this publication please use the final published version (if applicable).

Cover Page



Universiteit Leiden



The handle <http://hdl.handle.net/1887/18979> holds various files of this Leiden University dissertation.

**Author:** Usenko, Oleksandr

**Title:** Development and testing of the gravitational wave antenna MiniGRAIL in its full-featured configuration

**Date:** 2012-05-23

# Chapter 5

## SQUID detector for MRFM experiment

### 5.1 Introduction

In this chapter we present the first results of using the low noise SQUID amplifiers, we have developed for MiniGRAIL project, to detect a displacement of nanomechanical resonator used for magnetic resonance force microscopy (MRFM) experiment.

Currently, the most commonly used technique to detect the motion of ultrasensitive mechanical resonators is optical interferometry. Its applications range from Magnetic MRFM experiments [73], investigation of quantum effects in mechanical systems [74] and as we have already mentioned, gravitation wave experiments [5].

Unfortunately, despite the excellent sensitivity, the interferometric technique has a number of disadvantages:

- Optical detection becomes hard to implement when the size of the resonator is pushed to the nanoscale, because of the diffraction limit. For visible light wavelength one would in principle need a mirror of a few microns diameter, limiting the minimal width and the mass of a cantilever, while we are aiming to use cantilevers with diameters in order of a tenth of nm.
- When low or ultralow temperatures are required to reduce the thermal force noise, as for single spin MRFM, resonator heating due to light absorption is found to limit the effective cooling of the resonator [75]. This problem can be partially circumvented only by substantially reducing the input light power, at the price of reducing the displacement sensitivity.
- Excess heating caused by laser light might also be the cause of increased damping of the cantilever in a proximity of the sample surface, also called non-contact friction [76, 77, 78]. This effect is currently the limiting factor of MRFM sen-

sitivity. We hope that the fact that our force sensor allows operation at much lower temperatures can help to find ways to address this issue.

Other techniques have been recently demonstrated to be more compatible with ultralow temperatures. In particular, both Single Electron Transistors (SET) [79] and microwave cavities [80, 81, 82] have demonstrated outstanding displacement sensitivity for the detection of nanomechanical resonators at temperatures below 100 mK. So far, however, their implementation has been limited to systems where detector and resonator are tightly integrated, which is not practical for scanning probe applications like MRFM. Moreover, for microwave techniques the direct photon absorption still remains an issue at millikelvin temperatures, which again can only be mitigated by reducing the input power. Displacement sensors based on Quantum Point Contacts have also been demonstrated in an off-board setup [83], but so far their use has been limited to liquid helium temperature.

The SQUID-based technique we propose does not involve direct power dissipation in the resonator, and therefore is particularly suitable for ultralow temperature applications. Also, since the noise of the SQUID amplifier scales with temperature, the detection sensitivity should improve when going to ultralow temperatures. In practice however, due to reduced electron-phonon coupling (see section 3.5.4 in chapter 3), the SQUID noise saturates at  $T = 250 - 500$  mK so the signal-to-noise ratio will not improve below that temperature.

## 5.2 MRFM

In a conventional magnetic resonance imaging (MRI) detection scheme, the sample is placed in a strong homogeneous magnetic field  $B_0$  which results in Zeeman splitting between the nuclear spin states. The energy difference between the two states is

$$\Delta E = \gamma \hbar B_0, \quad (5.1)$$

where  $\gamma$  is the ratio of magnetic dipole moment of a spin to its angular momentum, called “gyromagnetic ratio”. If the sample is then exposed to a radio-frequency (rf) magnetic field with frequency that satisfies the condition

$$\omega = \frac{\Delta E}{\hbar} = \gamma B_0, \quad (5.2)$$

then the system absorbs energy from the rf radiation resulting in transitions between the nuclear spin states. From a classical point of view, the total nuclear magnetic moment of the sample starts changing its orientation. Once the rf field is turned off, any component of the total moment remaining perpendicular to the static field is left to precess about this field. The precession of this ensemble of nuclear magnetic moments produces a time-varying magnetic signal that can be detected with a pick-up coil. The electric current induced in the coil is then amplified and converted into a signal that is proportional to the number of nuclear moments (or spins) in

the sample. In MRI this signal can be reconstructed into a 3D image of the sample using spatially varying  $B_0$  field and Fourier transform techniques. While being a very powerful and widely used technique, Magnetic Resonance Imaging (MRI) has certain limitations. One of them is the minimal detectable number of spins resulting in a limit in volume resolution. Currently, the smallest volume element should contain  $\approx 10^{12}$  nuclear spins [84, 85] or  $\approx 10^6$  electron spins [86] for Nuclear Magnetic Resonance and Electron Spin Resonance microscopy respectively leading to a spacial resolution of a few microns.

By combining MRI with Probe Microscopy technology - MRFM technique is aimed for the ultimate MRI resolution improvement: detection of a single electron spin or even a single nuclear spin. So far a sensitivity, required to measure the single electron spin was already achieved by using an optical readout technique.[87]

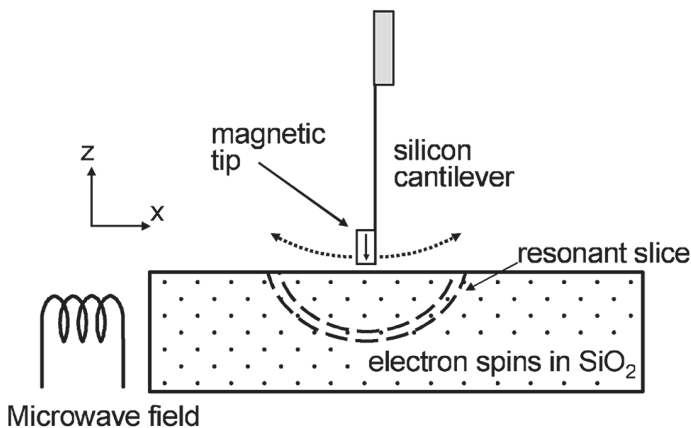


**Figure 5.1:** Scheme of MRFM experiment[88]

In an MRFM experiment, a magnetic particle mounted on the end of a cantilever generates a strong  $B_0$  field gradient (in order of  $10^5 - 10^6 T/m$ ). A microwave field excites the magnetic resonance in the region that satisfies the condition  $B_0(x, y, z) = \omega/\gamma$ , where  $\omega$  is the frequency of the RF field. The resonant region is confined to a thin, approximately hemispherical “resonant slice” around the magnetic particle. The radio frequency signal is modulated so that the spins are cyclically inverted at the cantilever’s mechanical resonance frequency, typically a few kHz. When modulated at resonance with the cantilever oscillation frequency, even the weak magnetic force induces detectable vibrations of the cantilever. By probing the resulting vibrational motion of the cantilever, it is in principle possible to detect spins with molecular or atomic resolution. By scanning the sample in 3D through this resonant region, a spatial map of the nuclear spin density can be made.

## 5.2.1 Sensitivity requirements

The interaction force between the tip and the spin is given by a dipole force which is proportional to the magnetic moment of the spin and the field gradient at the spin position. These forces are extremely small - the interaction force between a single electron spin and the magnetic tip is easily calculated to be as small as  $10^{-17}$  N. For a single proton the force is even smaller- in the order of  $10^{-20}$  N.

We can characterize the detection sensitivity of MRFM experiment in terms of a signal-to-noise ratio which is given by the ratio of the magnetic force due to the interaction with the spins to the force noise of the cantilever. For small volumes of spins, we measure statistical spin polarizations and the SNR is given by

$$SNR = N \frac{(\mu_N G)^2}{S_f \Delta f}, \quad (5.3)$$

where  $N$  is the number of spins,  $\mu_N$  is the magnetic moment,  $G$  is the  $B_0$  field gradient,  $S_f$  is the force noise spectral density of the cantilever and  $\Delta f$  is the measurement bandwidth, determined by the spin relaxation rate.

From equation (5.3) we see that the sensitivity of the nanomechanical resonators, used for MRFM experiments is limited by their force noise. According to the fluctuation-dissipation theorem, the power spectrum of the force noise power spectral density, acting on the cantilever is given by

$$S_f = \frac{4K_B T k}{Q \omega_0}, \quad (5.4)$$

where  $k$  is the cantilever spring constant,  $K_b T$  is the thermal energy,  $Q$  is the mechanical quality factor, and  $\omega_0$  is the resonance frequency. For a cantilever the ratio  $k/\omega$  is given by [89]

$$\frac{k}{\omega_0} \propto \frac{t^2 w}{l}, \quad (5.5)$$

where  $l$ ,  $w$ , and  $t$  are its length, width and thickness.

Thus the force noise of the cantilever can be reduced by achieving low operation temperature, high quality factor and by increasing the length of the cantilever and reducing the cantilevers width and thickness.

## 5.3 Experimental setup

### 5.3.1 Dilution refrigerator

Since we are aiming for continuous measurement at very low temperatures (as low as 10 mK, or even below 1 mK for the future MRFM experiments), the only option is a dilution refrigerator. We are using a commercial pulse-tube dilution refrigerator from Leiden Cryogenics [54]. Using the 2-stage pulse-tube cooler instead of a liquid helium bath and 1K pot greatly simplifies the maintenance and operation of the cryostat.

However this comes to a price with increased cool-down time and vibrations that the pulse tube induces on the mixing chamber. While, for our system, cool-down time is comparable to the one of a normal dilution refrigerator, the higher vibration level can be a problem for a vibration sensitive experiment like MRFM. To reduce the effect of mechanical vibrations, we have made some modifications both to the cryogenic and room temperature part of the cryostat. A general view of our experimental setup is

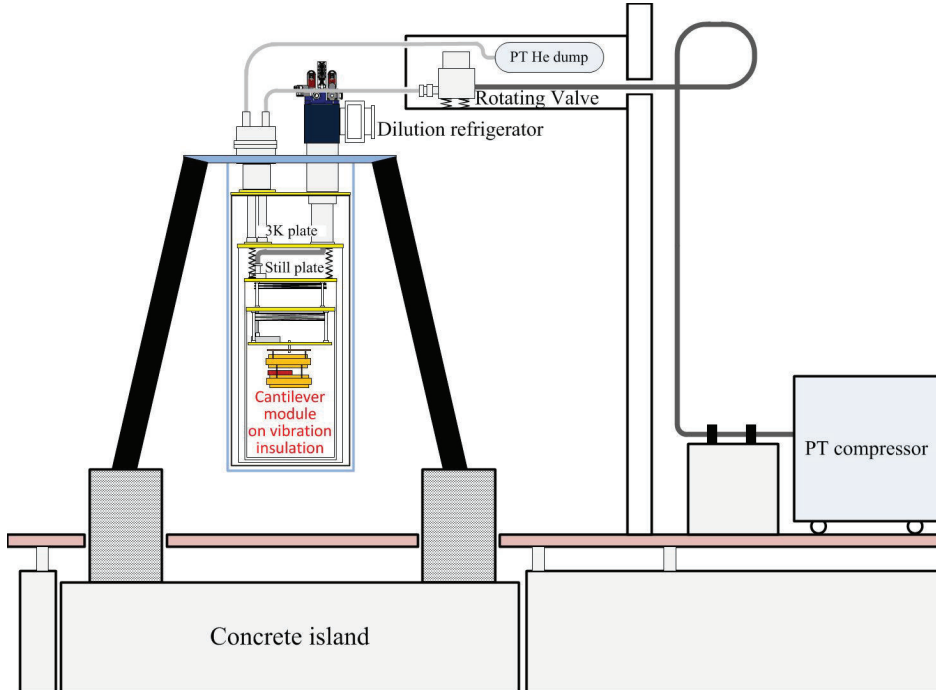


**Figure 5.2:** The scheme of the experimental setup. The cryostat is installed on a concrete island, which is mechanically decoupled from the rest of the laboratory building. The inner part of the cryostat, below the 3K plate, is suspended on a springs. Additional 2-stage mass-spring isolation system is installed below the mixing chamber.

shown on figure 5.2. Below we will describe the modifications we have made to each part.

### Room temperature modifications

To decouple the cryostat from the environment noise, it is installed on a vibration-free concrete island which is very well insulated from the rest of the building and from other experimental setups. The legs supporting the Dewar are filled with sand in order to increase their stiffness and damping. But, as we have found, the major source of external noise are the vibrations of the pulse-tube compressor and periodic



**Figure 5.3:** The rotating valve, suspended inside a box, attached to the wall of the laboratory. The periodic expansion of the tubes induces the motion of the valve, rather than pushing the PT head.

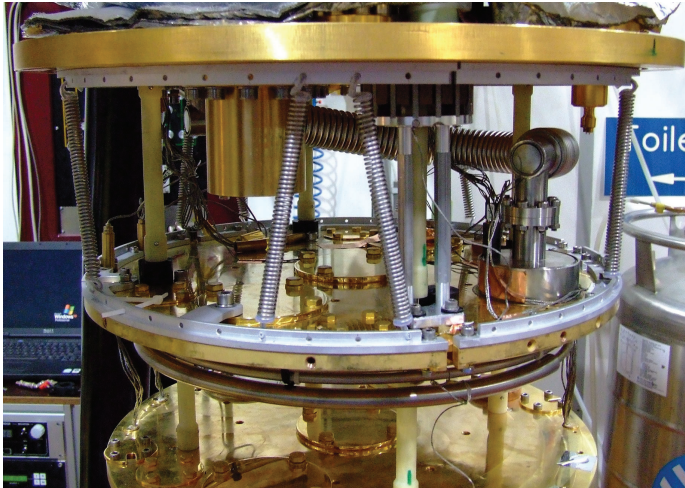
expansion of the flexible lines going from the compressor unit to rotating valve and from rotating valve to PT head. We have installed the compressor unit in the separate corridor behind the measurement hall and the long ( 20m) hoses, connecting it to the pulse-tube are attached to the concrete blocks. The rotating valve is freely suspended inside a box, attached to the wall (see figure 5.3), so that the expansion of the tubes induces the motion of the valve, rather than pushing the PT head. The box is also covered by acoustically insulating material in order to reduce the acoustic noise in the working space.

### Cryogenic part modifications

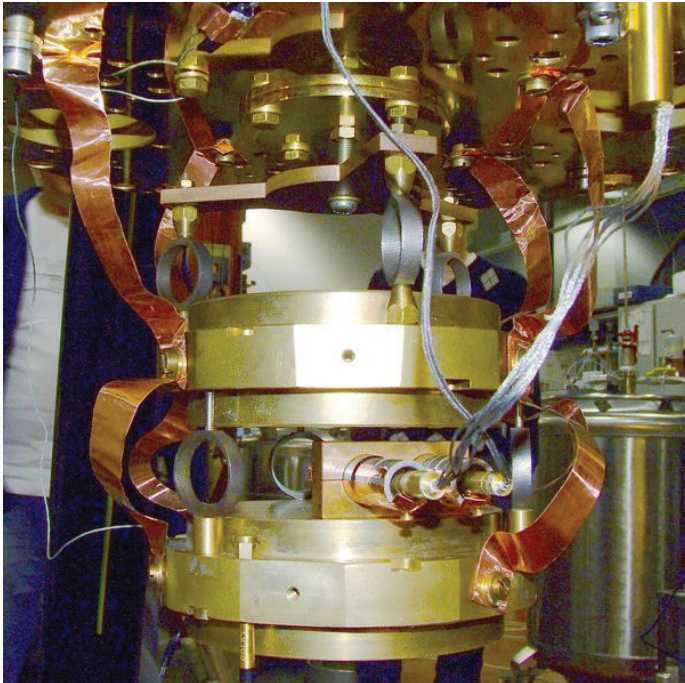
Even if the vibrations from room temperature part of pulse-tube are damped, there is still some vibration coming from the cold part of a PT itself. The frequency ranges from the base frequency of the pulse-tube of 1.4 Hz up to few kHz. The low frequency vibrations are induced by periodic expansion and contraction of thin stainless steel PT walls due to He gas pressure oscillations inside PT. High frequency ‘whistling’ comes from He flowing in the cold head and flexible hoses [90] and upconversion of low frequency vibrations, shaking the cryostat.

To reduce the vibrations to an acceptable level we have replaced the rigid links between 3K Plate and still plate with a spring suspension with resonance frequency of 3 – 5 Hz (figure 5.4(a)), depending on the suspended weight. Since the resonant frequency of the suspension is quite close to the pulse-tube frequency, we have also installed a magnetic damper to reduce the amplitude of vertical motion of the lower stage.

For further attenuation we have installed a vibration insulation consisting of 2 5 kg masses suspended on springs with a resonant frequency of 120 Hz. The total attenuation of the two masses system is calculated by Finite Element Analysis software to be above 100 dB in a frequency range 1-5 kHz. We measured an attenuation of



(a) 3K Plate - Still suspension



(b) Double mass-spring vibration insulation

**Figure 5.4:** Low temperature vibration insulation of the cryostat.

about 50 dB between the first mass and the mixing chamber, and a total attenuation of  $\geq 60$  dB in the frequency range of interest. (See figure 5.5).

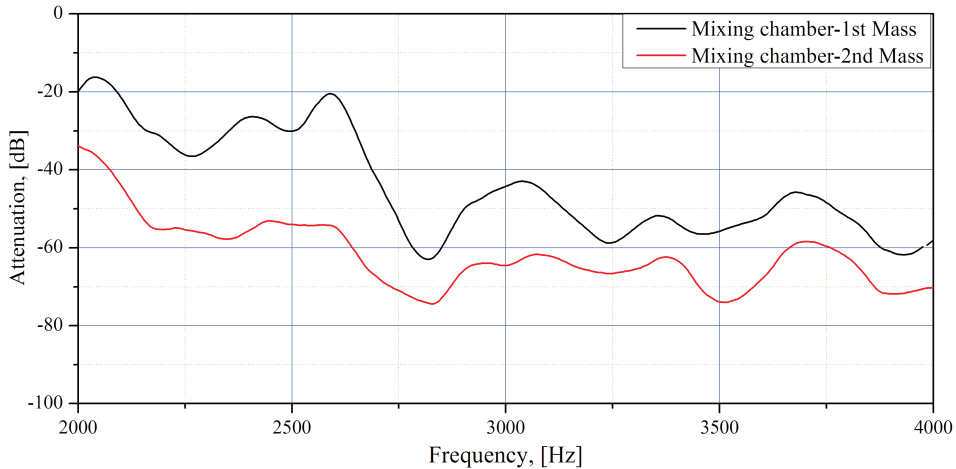


**Figure 5.5:** Mechanical attenuation between the mixing chamber and the two masses of vibration insulation measured at room temperature in air. The total attenuation of double mass system (red line) is above 60 dB in the frequency range of interest.

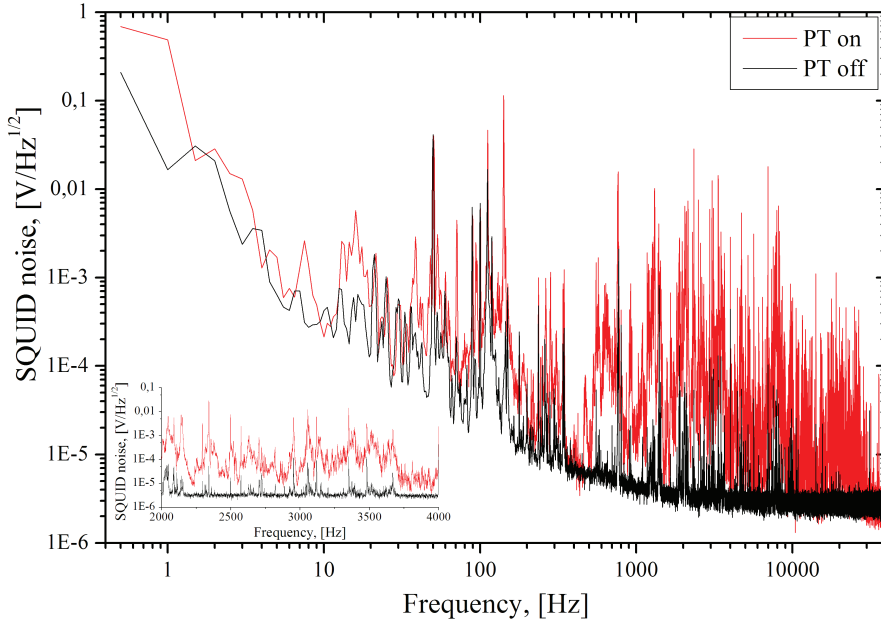
Since the experiment is now both mechanically and thermally decoupled from the mixing chamber, we need to provide a good thermal contact without degrading the vibration insulation. We used a soft commercial  $20 \times 0.2$  mm Cu tape, attached with the screws to a mixing chamber and the masses (see figure 5.4(b)). With the mixing chamber being at a temperature of 8 mK the gradient between the mixing chamber and the second suspension mass was less than 3 mK.

The noise spectral densities at the SQUID output of the original and modified cryostat are shown on figure 5.6. As we see even when the pulse-tube is turned off, the vibration insulation system significantly improves the insulation of the cryostat from the environmental mechanical vibrations. With PT on we hardly see any additional vibrational noise above the frequency of  $\sim 100$  Hz.

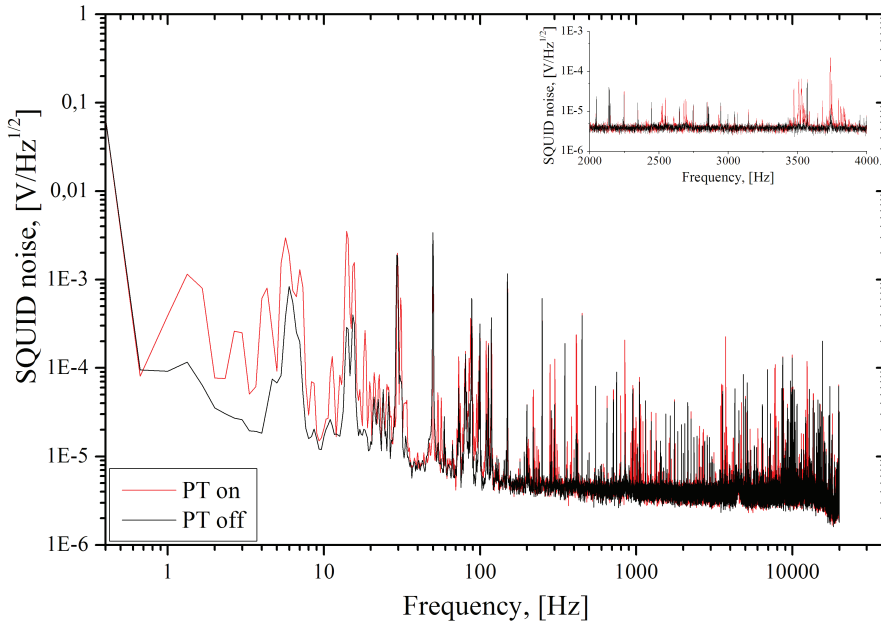
### 5.3.2 Cantilever chip

In our experiment, we have used two types of cantilevers.

The first one consisted of a  $50 - 70 \mu\text{m}$   $100 \text{ nm}$  thick SiC nanowire, attached to a Si AFM chip by means of electron induced Pt deposition. While, with this type of cantilever it is possible to make the resonator with optimal length, diameter and potentially very high quality factor [91], the cantilevers we have produced did not show any improvement in damping factor compared to the second type of cantilevers. That, combined with the extreme fragility, made us concentrate on the second type.



(a)



(b)

**Figure 5.6:** Vibrational spectral density measured by a SQUID on initial (a) and current (b) setup.

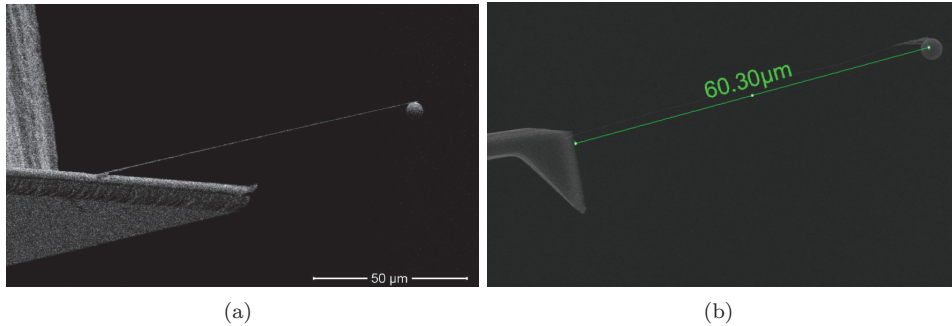


**Figure 5.7:** An electron microscopy image of the silicon resonator with a magnetic sphere attached to its end. (a)- the single crystal beam is 100 nm thick, 5  $\mu\text{m}$  wide and 100 nm long. The 4.5  $\mu\text{m}$  diameter magnetic sphere is made of a neodymium based alloy with remanence  $B_r = 0.75$  T. The frequency of the lowest flexural mode of the resonator is 3084 Hz, with a quality factor of  $3.8 \times 10^4$ . (b) - An AFM chip with 60.3 micron long, 100 nm diameter SiC nanowire with 3.6  $\mu\text{m}$  spherical magnet attached to its end.

The second type was a silicon resonator consisting of a 100 nm thick, 5  $\mu\text{m}$  wide and 100  $\mu\text{m}$  long single crystal beam, fabricated as reported in [92].

For both types we attached a 4 – 5  $\mu\text{m}$  diameter magnetic sphere of a Neodymium based alloy (MQP-S-11-9-20001-070 from Magnequench) to the end of the resonator using a nano-manipulator inside an electron microscope [93], and magnetized it in a 3 T field at room temperature. The alloy has a nominal remanence field  $B_r = 0.75$  T, and the estimated magnetic moment of the magnetized particle is  $\mu = 2.8 \times 10^{-11}$  J/T.

Mechanical properties of two types of cantilevers are summarized in table 5.2

	Si beam	SiC nanowire
Length, [ $\mu\text{m}$ ]	$\sim 100$	50 – 70
Width [ $\mu\text{m}$ ]	5	0.1
Thickness, [ $\mu\text{m}$ ]	0.1	0.1
Spring constant, [N/m]	$1.5 \times 10^{-4}$	$2 - 5 \times 10^{-5}$
Magnet diameter, [ $\mu\text{m}$ ]	4 – 5	4 – 5
Resonant frequency, [kHz]	$\sim 3$	1.5 – 2
Quality factor @ 4.2 K	$3 \times 10^4$	$1 \times 10^4$
Damping, [Nm/s]	$\sim 10^{-13}$	$\sim 10^{-13}$

**Table 5.1:** Summarized properties of cantilever and detection chain parameters

### 5.3.3 Cantilever module

The cantilever module is made similar to the SQUID modules used in MiniGRAIL project[25](see figure 5.8). The cantilever, pickup and calibration coils are mounted on the pc-board fixed on a lead-plated copper holder. Nb can with CryoPerm foil around it provide a magnetic shielding. The pickup coil is connected to a SQUID module with Nb braided twisted pair superconducting wire.

The resonator is placed at about  $10\ \mu\text{m}$  above the edge of the detection coil. The silicon chip supporting the resonator is held in position and thermally anchored to a copper holder by a brass spring. The detection coil has square geometry with 22 windings, a width of  $670\ \mu\text{m}$  and an estimated inductance of  $0.6\ \mu\text{H}$ . The coil is connected to the input coil of a two-stage SQUID amplifier, made of a commercial Quantum Design sensor SQUID and a flux transformer dc SQUID. The SQUID is operated with commercial direct readout electronics from Star Cryoelectronics. We have also placed a small piezo crystal inside the module to be able to excite the cantilever mechanically.

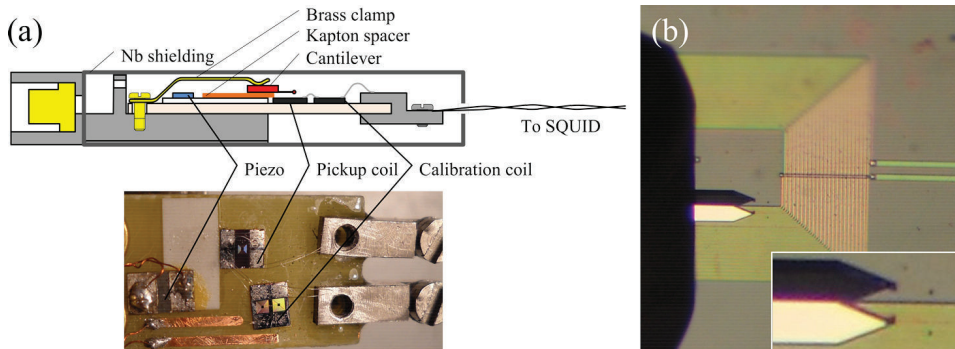


**Figure 5.8:** (a) - Cantilever module. (b) - Cantilever chip with a SiC nanowire resonator aligned above the inner edge of a detection coil. The small dark dot to the right of the AFM chip is the magnetic particle.

### 5.3.4 Detection scheme

The idea of the experiment is very simple and is shown on figure 5.9 A cantilever with a small magnetic particle, attached to its end, is placed at a close distance ( $20\text{--}50\ \mu\text{m}$ ) from a superconducting pickup coil, coupled to a squid. The motion of a magnetic particle results in a change of magnetic flux in the coil and induces the current which is measured by the SQUID. The calibration coil is used to measure the coupling between the Cantilever and the pickup coil (see section 5.5).

Parameter	Value
Pickup coil inductance, $L_p$	600 nH
Pickup coil size (IDxOD)	230x670 $\mu\text{m}$
Pickup coil number of turns	2x22
Pickup coil linewidth	2 $\mu\text{m}$
Calibration coil inductance, $L_{cal}$	18 nH
Calibration coil mutual inductance, $M_{cal}$	15 nH
SQUID input coil inductance, $L_i$	1.6 $\mu\text{H}$
SQUID input coil mutual inductance, $M_i$	10 nH

**Table 5.2:** Summarized properties of cantilever and detection chain parameters

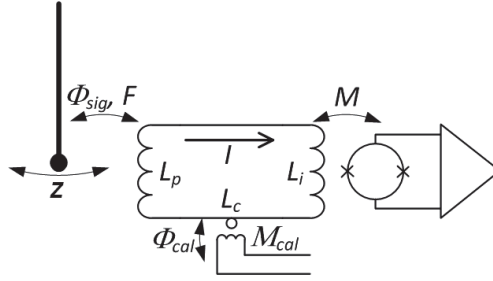


**Figure 5.9:** Scheme of cantilever motion detection using SQUID read out.

## 5.4 Optimizing the sensitivity

In order to optimize the coupling between the magnetic particle and a pickup coil we need to find a position where the motion of the magnetic particle with dipole moment  $\mathbf{m}$  in a given direction  $(x, y, z)$  results in the maximum flux change ( $\phi_x = \frac{\delta\phi}{\delta x}, \phi_y = \frac{\delta\phi}{\delta y}, \phi_z = \frac{\delta\phi}{\delta z}$ ) in the pickup coil.

We calculate the flux generated by the magnetic dipole in the coil by solving the inverse problem - by calculating the magnetic field  $\mathbf{B}$  and its gradients  $\Delta B_x, \Delta B_y, \Delta B_z$  at the position of a magnetic particle, generated by current ( $I_c$ ) in the pickup coil. A magnetic dipole can be modelled as a small current loop, with Area  $\mathbf{A}$  and a current  $i$ . Dipole moment of such a loop will be

$$\mathbf{m} = i\mathbf{A} \quad (5.6)$$

Magnetic flux ( $\phi_c$ ) induced in the pickup coil by a current loop and magnetic flux induced in the loop by a current in the coil ( $I_c$ ) are:

$$\phi_c = iM \quad (5.7)$$

$$\phi_l = I_c M, \quad (5.8)$$

where  $M$  is the mutual inductance between the current loop and the pickup coil, then

$$\phi_c = \frac{i\phi_l}{I_c} = \frac{iA\frac{\phi_l}{A}}{I_c} = \mathbf{m} \frac{\mathbf{B}}{I_c}, \quad (5.9)$$

where  $\mathbf{B}$  is the magnetic field at dipole position.

For the current layout of the experiment the magnetic particle is magnetized in the direction of its motion, perpendicular to the coil plane, so we are only interested in the sensitivity in the  $z$  direction:

$$\phi_z = \mathbf{m} \frac{\partial B_z}{\partial z}. \quad (5.10)$$

The magnetic field  $B$ , generated by the pickup coil, can be calculated by using the Biot-Savart law:

$$\mathbf{B} = \frac{\mu_0}{4\pi} \int \frac{I_c d\mathbf{l} \times \mathbf{r}}{r^3}, \quad (5.11)$$

where  $d\mathbf{l}$  is a vector, whose magnitude is the length of the differential element of the wire, and whose direction is the direction of current,  $\mathbf{B}$  is the net magnetic field,  $\mu_0$  is the magnetic constant,  $\mathbf{r}$  is the full displacement vector from the wire element to the point at which the field is being computed.

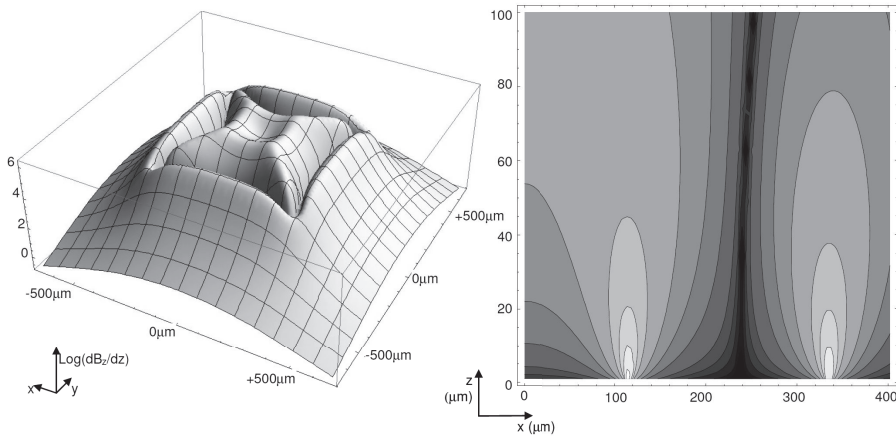


**Figure 5.10:** Left: position sensitivity of pickup coil to the magnetic dipole located at  $50 \mu\text{m}$  above the coil surface. Right: cross-section of the sensitivity plot with the  $y$ -plane. [94].

To simplify the calculations the pickup coil is approximated by a single loop, with uniform current density. The coil is placed in the  $(x,y)$  plane. The dipole is parallel to  $z$  axis.

The results of a calculation of the vertical gradient of the field  $\frac{\partial B_z}{\partial z}$  versus the position of the cantilever above the coil is shown on figure 5.10. The vertical distance between the cantilever and the pick-up coil is set to 50  $\mu\text{m}$ .

## 5.5 Measuring the Cantilever Coupling

### 5.5.1 Cantilever-SQUID calibration

In order to estimate the force noise of the cantilever we need to measure how effective does the cantilever motion converts to a current in the SQUID pickup coil. In other words, we have to measure  $\phi_z$  from equation 5.10. We consider the same layout as in the previous sections: the pickup coil and the cantilever are placed parallel to the  $xy$  plane, and we detect the motion of the magnetic particle in  $z$  direction.

The calibration procedure is similar to the one we have used to calibrate MiniGRAIL modes coupling in the previous chapter. We have inserted a small transformer between the detection and the SQUID input coil. The inductance of the secondary coil of the calibration transformer  $L_C$  is made small enough not to contribute to the total inductance of the detection loop. Since the magnetic flux through the superconducting loop is preserved, the injected calibration flux  $\Phi_{cal}(\omega)$  will generate a change in the screening current  $I$ . The force, acting on the cantilever in the  $z$  direction from a magnetic field  $B$ , generated by the screening current in the pickup coil is given by

$$F = \mathbf{m}\nabla B_z \equiv \phi_z I \quad (5.12)$$

We can write a set of equations describing the cantilever behaviour:

$$\begin{cases} \Phi_{cal} + \Phi_{sig} + L_{tot}I = 0 \\ (-\omega^2 + \frac{i\omega_0}{Q}\omega + \omega_o^2)z = \frac{F+F_{th}}{m} \approx \frac{F}{m} \end{cases} \quad (5.13)$$

The first equation represents the magnetic flux conservation in a superconducting loop.  $L_{tot} \equiv L_p + L_i + L_c + L_{par}$  is the total inductance of the pickup loop including the unknown parasitic inductance  $L_{par}$ .  $\Phi_{sig}$  is the flux that cantilever motion induces in the pickup coil. The second equation is the standard equation of motion of a driven harmonic oscillator. In principle, we should take into account both the force  $F$  due to the calibration current and a thermal noise force  $F_{th}$ , but we consider the calibration signal to be high enough to dominate in the system, and ignore any other force sources. Since  $F = \phi_z I$  and  $\Phi_{sig} = \phi_z z$  we can write the set of equations of motion in the following form

$$\begin{cases} \Phi_{cal} + \phi_z a + L_{tot}I = 0 \\ z = \frac{\phi_z I}{m(-\omega^2 + \frac{i\omega_0}{Q}\omega + \omega_o^2)}. \end{cases} \quad (5.14)$$

These equations can be solved for  $z(\omega)$  and  $I(\omega)$

$$\begin{cases} z(\omega) = -\frac{\phi_z \Phi_{cal}}{mL_{tot}(-\omega^2 + i\frac{\omega_0}{Q}\omega + \omega_0^2 + \frac{\phi_z^2}{mL_{tot}})} \\ I(\omega) = -\frac{\Phi_{cal}}{L_{tot}(1 + \frac{\phi_z^2}{mL_{tot}(-\omega^2 + i\frac{\omega_0}{Q}\omega + \omega_0^2)})} \end{cases} \quad (5.15)$$

where  $I_{cal} = \frac{\Phi_{cal}}{L_{tot}}$  is the current in the input loop due to the calibration flux. From the first equation we see that the cantilever response to the calibration signal is Lorentzian with the coupling to the detection coil introducing frequency shift due to an additional magnetic spring constant. It can be easily shown that for high  $Q$  and a small relative change of the resonant frequency, the first equation corresponds to a harmonic oscillator with the resonant frequency of  $\omega_0'^2 \equiv \omega_0^2 + \frac{\phi_z^2}{mL_{tot}}$  and a spring constant of  $k' = k + \frac{\phi_z^2}{L_{tot}}$ .

By further simplifying the second part of equation (5.15) we get an expression for frequency dependence of the current in the detection loop:

$$I(\omega) = -\frac{-\omega^2 + i\frac{\omega_0}{Q}\omega + \omega_0^2}{-\omega^2 + i\frac{\omega_0'}{Q}\omega + \omega_0'^2} I_{cal} \quad (5.16)$$

Similar to what we did in section 4.2.1, we can define a coupling factor  $\beta$  as

$$\beta^2 = \frac{\omega_0^2 - \omega_0'^2}{\omega_0'^2} \equiv \frac{\phi_z^2}{k' L_{tot}} \quad (5.17)$$

Since we can experimentally measure only a coupled resonant frequency  $\omega'$ , we write down the final expression for the current as

$$I(\omega) = -\frac{-\omega^2 + i\frac{\omega_0'}{Q}\omega + \omega_0'^2(1 - \beta^2)}{-\omega^2 + i\frac{\omega_0'}{Q}\omega + \omega_0'^2} I_{cal} \quad (5.18)$$

Now, we can determine the coupling factor  $\beta^2$  and thus  $\phi_z$  by accurately measuring the calibration transfer function  $I(\omega)$  vs  $\phi_{cal}$  with the lock-in amplifier and fitting with equation (5.18). An interesting point is that the factor  $\beta^2$  affects only the shape of the transfer function, in particular it is related with the difference between resonance and antiresonance frequencies in equation (5.18). Thus, the estimation of  $\beta^2$  is completely unaffected by any uncertainty on the absolute value of the calibration flux  $\Phi_{cal}$ , the SQUID gain or the total loop inductance value  $L_{tot}$ . One can also show that  $1 - \beta^2$  is the ratio of the values of the transfer function well below and well above the resonance frequency, and that, in the limit of small  $\beta^2$  and high  $Q$ , the ratio between maximum and minimum of the module of the transfer function is given by  $1 + \beta^2 Q$ .

The calibration curves for the first two normal modes of the cantilever are shown on figure 5.11.

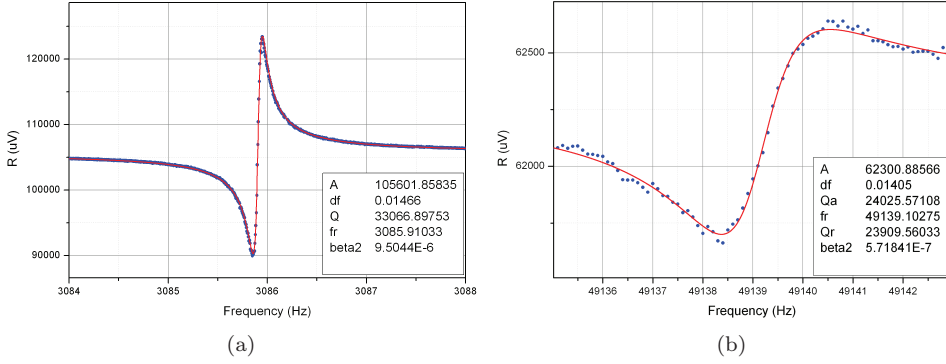


**Figure 5.11:** Calibration of cantilever-SQUID coupling for the first two fundamental modes of the cantilever.

## 5.5.2 Thermal Noise

After we have measured the coupling, we can estimate the equivalent temperature  $T_{eq}$  of the cantilever vibration mode. If it is only excited by the thermal noise then the cantilever displacement with the variance of

$$\langle z_{th}^2 \rangle = \frac{4K_B T_{eq}}{k'} \quad (5.19)$$

would result in a current in the detection loop which is given by

$$\langle I_{th}^2 \rangle = \frac{\phi_z^2}{L_{tot}^2} \langle z_{th}^2 \rangle = \frac{\phi_z^2 4K_B T_{eq}}{k' L_{tot}^2} = \beta^2 \frac{4K_B T_{eq}}{L_{tot}} \quad (5.20)$$

The voltage noise on the output of the SQUID is:

$$S_V = M^2 \langle I_{th}^2 \rangle V_{\Phi}^2 = 4K_b \frac{M^2}{L_{tot}} \beta^2 V_{\Phi}^2 T_{eq} \equiv A T_{eq}, \quad (5.21)$$

where  $V_F$  is the flux gain of the SQUID and  $A \equiv 4K_b \frac{M^2}{L_{tot}} \beta^2 V_{\Phi}^2$  is a conversion factor from the equivalent temperature of the mode to a voltage at the output of the SQUID. The equivalent temperature of the cantilever mode is not necessarily equal to the thermodynamic temperature. It can be higher if the cantilever is excited by some other noise sources, like mechanical vibration.

Note that the above expressions contain the total inductance  $L_{tot}$ , which is unknown. However, we can estimate the relation  $\frac{M^2}{L_{tot}}$  by measuring the thermal noise spectrum of a resistor connected in series with  $L_{tot}$ . In our case we can use the resistance of Al bonding wires in the cantilever module. Above the superconducting transition temperature of Al ( $T_c \approx 1.17$  K) the bonding wires generate thermal noise, with power spectral density given by:

$$S_{vv} = 4K_bTR \quad (5.22)$$

The impedance of the series RL circuit is  $Z(\omega) = R + i\omega L$ , so the noise at the output of the SQUID is:

$$S_{V_{out}}(\omega) = \frac{S_{vv}}{|Z|^2} M^2 V_{\Phi}^2 = \frac{4K_bTRM^2V_{\Phi}^2}{(R^2 + \omega^2L_{tot}^2)} \equiv \frac{4K_bTM^2V_{\Phi}^2}{R(1 + \omega^2\frac{L_{tot}^2}{R^2})} \quad (5.23)$$

The noise spectra in equation (5.23) can be fitted with a simple function:

$$S_V(f) = \frac{S_0}{1 + \frac{f^2}{f_0^2}}, \quad (5.24)$$

where  $S_0 = \frac{4K_bTM^2V_{\Phi}^2}{\Phi_0 R}$  is the thermal noise of the resistor and  $f_0 = \frac{R}{2\pi L}$  - the cutoff frequency of RL lowpass filter.

We can get the expression for  $\frac{M^2}{L_{tot}}$ :

$$\frac{M^2}{L} = \frac{\pi\Phi_0 S_0 f_0}{2k_bTV_{\Phi}^2} \quad (5.25)$$

An example of a SQUID noise spectra at  $T = 1246$  mK and the fit are shown on figure 5.12

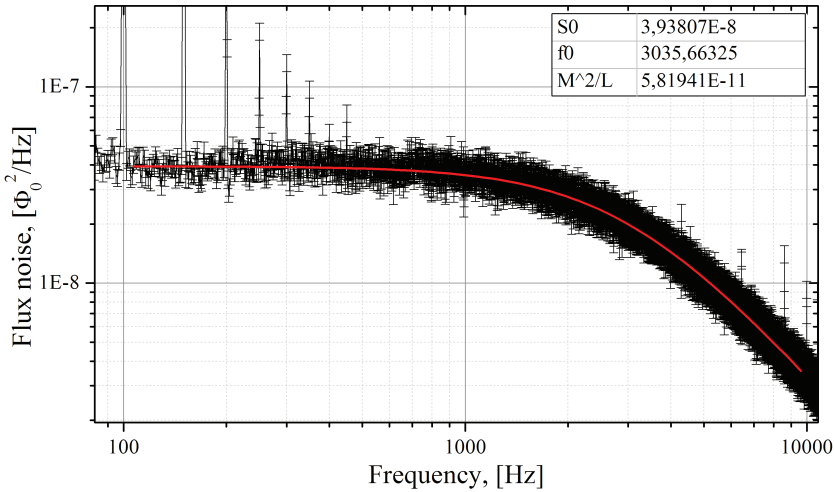


**Figure 5.12:** Calibration of the SQUID input loop.  $T=1246$  mK

## 5.6 Experimental results

We have performed a series of cooldowns (runs) in a dilution refrigerator. During these runs we were focused on reducing the vibration noise and improving the thermalization of the cantilever chip in order to improve the force sensitivity of the resonator. The cantilever and SQUID modules were placed on the second mass of vibration isolation stage. During the cooldown we have reached the minimal temperature of the mass of about 9 mK. The flux noise of our 2-stage SQUID amplifier scaled down with temperature to about 500 mK, reaching a constant level of  $\sim 0.6 \mu\phi_0/\sqrt{\text{Hz}}$ .

First, in order to determine the properties of the cantilever at low temperature, we have mechanically excited it with the small piezo oscillator in the cantilever module and measured the ringdown signal with the lock-in amplifier. We have found that we can also see the second vibrational mode of the resonator in the SQUID bandwidth.

Mode	$f_0, [\text{Hz}]$	Q	$\beta$
1.	3084	$3.8 \times 10^4$	$9.5 \times 10^{-6}$
2.	49150	$2.3 \times 10^4$	$5.7 \times 10^{-7}$

**Table 5.3:** Properties of first two cantilever modes at low temperature.

As we can see, the second mode has a coupling almost 20 times smaller than the first one because the cantilever position was optimized for the first mode only. However, its thermal noise was still visible in the SQUID noise spectra up to the lowest temperature.

After we have characterized the modes we have measured the effective temperature of the resonator by stabilizing the dilution refrigerator, recording its temperature with a calibrated thermometer and measuring the energy stored in the modes. The power spectral density of the SQUID output signal, featuring the Lorentzian peak due to the thermal motion of the resonator at two separate bath temperatures is shown in the right side of figure 5.13. The measured spectral density is very well fitted by a sum of the white noise of the SQUID and Lorentzian shape, indicating that the modes are likely excited by the wideband thermal noise rather than coupling to narrowband vibrational peaks.

The area of the Lorentzian peak is proportional to the mean resonator energy and can easily be converted to the effective temperature of the mode using the equation (5.21). The effective noise temperature  $T_N$ , plotted as a function of the thermal bath temperature  $T$ , is shown in the left side of figure 5.13. The difference between “Run6” and “Run8” data is in improved thermalization of the cantilever chip by means of a brass clamp. For “Run8” data a remarkable agreement between the resonator noise temperature and the bath temperature is observed at temperatures from 1 K down to about 30 mK. The noise temperature is then found to saturate at about 25 and 20 mK for the first and the second modes respectively, suggesting that some residual power dissipation, combined with the exceedingly small thermal conductance at millikelvin temperature, is limiting further cooling of the resonator.

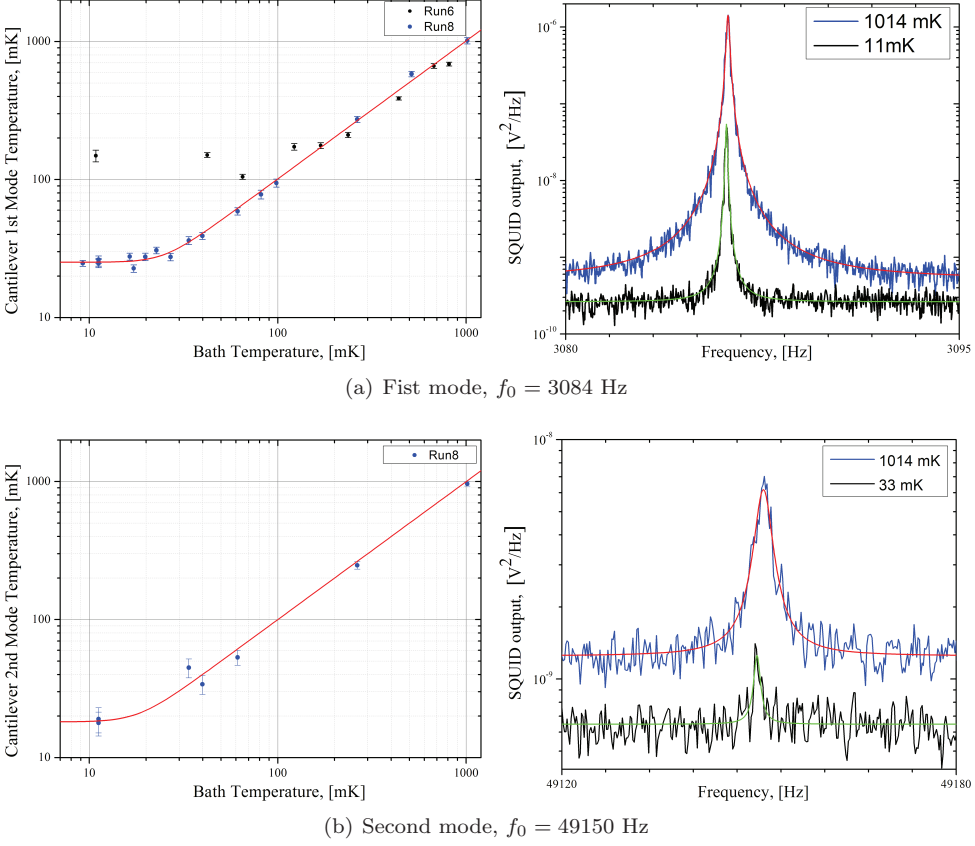


**Figure 5.13:** Left: effective temperature of first (a) and second (b) fundamental modes of the cantilever versus thermodynamic temperature. The continuous red line represents a fit to the data with a standard saturation curve, yielding a saturation temperature  $T_{0_1} = 25 \pm 1$  mK for the first mode and  $T_{0_2} = 18 \pm 3$  mK for the second one. Right: power spectral density of the SQUID output at two different bath temperatures, featuring the Lorentzian peak due to the resonator thermal motion.

The red line presents a fit to the data of the form  $T_N = (T^n + T_0^n)^{1/n}$ , where  $T_0$  is the saturation temperature and the exponent  $n$  is determined [57] by the temperature dependence of the limiting thermal resistance which scales as  $T^{-(n-1)}$ . For the first mode the fit yields a saturation temperature  $T_0 = 25 \pm 1$  mK, while the exponent  $n = 5 \pm 2$  is consistent with a limiting thermal resistance due either to a boundary effect or to a 2D or 3D phonon gas [57]. For the second mode the fitted saturation temperature is  $T_0 = 18 \pm 3.5$  mK, but the SNR was too low to produce any consistent result for the value of the exponent.

Assuming that the saturation is due to power dissipation in the silicon resonator, and using a simple 3D phonon model to estimate the thermal resistance through the resonator beam, we find that the residual power required to explain the observed saturation is of order 100 aW. Such power could be related with microwave dissipation in the magnetic sphere, due either to the Josephson radiation from the SQUID or to microwave thermal radiation from room temperature wiring. By means of a careful engineering of microwave filters, so far not implemented, it should be possible to suppress the residual power by several orders of magnitude, and to cool the resonator to even lower temperatures.

Regardless of the low-temperature noise saturation, the force noise amplitude spectral density can still be calculated using the fluctuation-dissipation formula  $F_{min} \equiv \sqrt{S_F} = \sqrt{4k_B T_N \gamma}$ , where  $\gamma = k/(2\pi f_0 Q)$  is the damping constant of the resonator. In the saturation region, where  $T_N = T_0$ , we obtain a minimum force noise spectral density  $F_{min} = 0.51 \pm 0.03$  aN/ $\sqrt{\text{Hz}}$ , close to the best values ever reported in literature [81].

We can also estimate the displacement sensitivity of our detection scheme by converting the mean energy of the resonator  $k_B T_N$  into mean displacement fluctuations  $\langle x^2 \rangle = k_B T_N / k$ . From this we infer that the experimental SQUID white noise corresponds to an equivalent displacement noise of 8 pm/ $\sqrt{\text{Hz}}$ . This figure is comparable with that of other techniques used with cryogenic micron-sized or nanomechanical resonators, like ultralow power interferometry [75] or quantum point contacts [83]. We note, however, that the displacement sensitivity can be greatly enhanced, by at least two orders of magnitude, by means of relatively straightforward improvements. The coupling between the magnetic particle and the detection coil can be substantially increased by reducing the size of the coil to a few microns. In this case, a possible issue could be the direct pick-up of magnetic noise due to magnetization fluctuations of the ferromagnetic particle. Furthermore, the SQUID noise can be improved at least by a factor of 2 by using either better conventional dc SQUIDs [95] or by implementing recently developed SQUID magnetometers based on non-dissipative inductive readout, exhibiting quantum limited sensitivity [96].

### 5.6.1 Conclusions and further experiment development

In conclusion, we have developed a SQUID-based technique suitable for detecting the displacement of a nanomechanical resonator at ultralow temperatures. By assembling a relatively simple experimental setup and cooling a silicon resonator to an effective temperature of 25 mK, we achieved a force noise spectral density of  $0.51 \pm 0.03$  aN/ $\sqrt{\text{Hz}}$ . We believe that by substantially improving the experimental setup, in particular the electromagnetic shielding, the effective resonator temperature can be further reduced, possibly down to sub-millikelvin temperatures. The only fundamental limit appears to be the backaction noise of the SQUID amplifier. However, we estimate that this will not be an issue until temperatures as low as 100  $\mu\text{K}$  are reached.

To illustrate the potential of the measured force sensitivity in application to

MRFM experiment, we calculate that a force of 0.03 aN is generated by a single proton spin flipping in a field gradient of  $2 \times 10^6$  T/m (e.g. at 50 nm from a 1  $\mu$ m diameter magnet with a magnetization of 0.75 T). While with a low force noise of only 0.1 aN/ $\sqrt{\text{Hz}}$ , a force from a single proton would in principle be detectable in an averaging time of less than 10 seconds, the current force sensitivities of MRFM are limited by non-contact friction. We hope that the fact that our force sensor allows operation at much lower temperatures can help to find ways to address this issue.

Our detection technique is also naturally suitable for detecting the motion of nanowire resonators, which pose even harder problems for interferometric detection due to their low reflectivity [97]. Force sensors based on ultrathin nanowires can in principle reach unprecedented force sensitivity. For example, single crystal SiC nanowires have demonstrated a damping factor as low as 4 fNm/s at room temperature [91], which would yield a force noise spectral density below 0.1 aN/ $\sqrt{\text{Hz}}$  at 10 mK.

There is, however, an obvious limitation on the strength of magnetic fields used in the experiment to be lower than the critical field of the superconducting detection coil. For the thin film Nb coils we use, this means a maximal field of  $\sim 200$  mT can be applied. In fact this value is close to the magnetic field on the surface of the magnetic particle attached to the mechanical resonator. This, however, need not preclude the low field magnetic resonance imaging experiments. We also note that the SQUID itself is spatially separated from the detection coil and is not affected by the externally applied magnetic field.

The future development of this experiment is quite straightforward. A new detection coil with sensitivity optimized geometry and integrated rf line has been designed and made [98], allowing to generate an rf field for magnetic resonance experiments. A 3D scanning stage for spacial spin imaging is also being developed.

A first MRFM experiment, utilizing a SQUID detection scheme, a new detection coil and a vertical scanning stage is reported in [99]. We have found a clear evidence of cantilever coupling to paramagnetic spin system, located at  $Si - SiO_2$  boundary of the detection coil substrate.

